DNA Vibrational Coupling Revealed with Two-Dimensional Infrared Spectroscopy: Insight into Why Vibrational Spectroscopy Is Sensitive to DNA Structure

Amber T. Krummel and Martin T. Zanni*

Department of Chemistry, University of Wisconsin−Madison, Madison, Wisconsin 53706-1396

Received: April 27, 2006

Two-dimensional infrared (2D IR) spectroscopy was used to study the carbonyl vibrational modes of guanine and cytosine bases in A- and B-form DNA. Located between 1600 and 1700 cm^{-1}, these modes are often used to monitor DNA secondary structure with traditional infrared spectroscopies such as FTIR, but traditional spectroscopies lack the necessary observables to unravel the coupling mechanisms that make these modes sensitive to secondary structure. By using 2D IR spectroscopy and electronic structure calculations on $d(G_5C_5)$ and $d(GC)_8$ model nucleic acids, we find that hydrogen-bonded guanine/cytosine base pairs are primarily electrostatically coupled and that the coupling between these modes can be modeled with a transition dipole density approach. In comparison, electrostatics is insufficient to model stacked bases because of cooperative charge-sharing effects, but the coupling can be accurately calculated using a finite difference method. We find that the coupling is very strong for both hydrogen-bonded and stacked base geometries, creating vibrational modes that extend both across the base pairs and along the lengths of the helices. Our results provide a physical basis for understanding how strong coupling gives rise to the empirically established relationship between infrared spectroscopy and DNA/RNA secondary structure.

Introduction

Infrared spectroscopy is often used to monitor DNA and RNA structure and kinetics. Although IR spectroscopy does not provide the same level of atomic detail that X-ray crystallography or NMR spectroscopy do, it still remains widely used because it can distinguish between A-, B-, and Z-form double helices, triple stranded helices, various base pairing motifs such as Hoogsteen and reverse Hoogsteen, and other structural motifs.[1−5] Furthermore, little sample material is required, spectra can be collected rapidly, and the samples can be immersed in liquids, membranes, solids, or on surfaces. These features are often exploited to study DNA and RNA secondary structure changes upon drug binding, thermal denaturation and folding, protein complexation, and surface adherence, for instance.[4−8] But despite the widespread use of FTIR spectroscopy, the correlation between DNA spectral features and oligomer structure remains empirical because the underlying forces that link the IR spectral features to the details of the molecular structures are not understood. By focusing on the carbonyl stretches of DNA oligomers composed of guanine and cytosine bases, we use two-dimensional infrared (2D IR) spectroscopy and electronic structure calculations to explore this link and better understand the physical basis that makes IR spectroscopy a useful probe of DNA/RNA secondary structure.

Previous FTIR isotope labeling studies and vibrational circular dichroism (VCD) experiments on the carbonyl stretches of DNA and RNA oligomers point to coupling as the reason that IR spectroscopy is sensitive to oligomer secondary structure. This conclusion seems reasonable considering that IR spectroscopy can be used to monitor protein secondary structure because the carbonyl stretches along the protein backbone (amide I modes) are strongly coupled.[9] However, the two proposed DNA coupling models are at odds with one another; the FTIR experiments can be interpreted with a model that only includes coupling between bases in base pairs without any need for coupling between stacked bases,[10] whereas the VCD experiments can be simulated with a model that only requires coupling between stacked bases.[11,12] This disagreement in interpretation arises because these traditional IR spectroscopies do not contain enough observables to distinguish between base pair versus stacked couplings, making it difficult to develop and test coupling models.

Two-dimensional IR spectroscopy is a much better method for testing coupling models.[13−17] Besides improving the resolution by spreading the IR spectra into two dimensions, 2D IR spectroscopy also provides coupling information through cross-peak intensities and frequencies, similar to cross-peaks that arise in 2D NMR between coupled spins. Although a relatively new technique,[14,15,17−30] it has already proven valuable for testing and developing coupling models of proteins.[13−17] In the pulsed version of 2D IR spectroscopy,[31,32] multiple femtosecond infrared pulses are used to coherently excite molecular vibrations, creating a signal that is analogous to the free-induction decay emitted in NMR spectroscopy, but instead contains information on the vibrational couplings, relative bond orientations, fast kinetics, and infrared line shapes of the system under study.[15,18,19,33] Furthermore, the polarizations of the pulses can be utilized to independently determine the relative angles between coupled transition dipoles, another observable that is very sensitive to coupling.[19] In the work presented here, the cross-peaks in the 2D IR spectra provide the additional observables necessary to ascertain a coupling model that includes both base pairing and stacking couplings.

In the following, we focus on two model oligomers: double-stranded $d(G_5C_5)$ and $d(GC)_8$ deoxyribonucleic acids. $d(GC)_8$ has alternating stacked G and C bases and is in the B-form, while $d(G_5C_5)$ is similar to poly(dG)−poly(dC) and is in the A-form.[34−37] The 2D IR spectra of these oligomers are distinct, exhibiting different peak frequencies, intensities, shapes, and cross-peaks. By utilizing the improved resolution and informa-

* Corresponding author. E-mail: zanni@chem.wisc.edu.

10.1021/jp062597w CCC: $33.50
Published on Web 06/22/2006

tion content of 2D IR spectroscopy, we determine the couplings between the bases from simulations of the spectra and electronic structure calculations. These two sequences were chosen because both have Watson−Crick base pairing but should presumably have different stacking geometries. In fact, we find that the base pair coupling is the same for both strands. In contrast, the coupling between stacked bases varies widely depending on the sequence and secondary structure. An analysis of the coupling using a series of increasingly sophisticated models indicates that base pair coupling can be modeled with transition dipole density distribution, which suggests that the coupling between these bases is mostly electrostatic. In contrast, electrostatic models do not work for stacked bases because a small amount of charge transfer occurs. From our results, we conclude that IR spectroscopy is sensitive to DNA and RNA secondary structure because of *both* strong base pair and strong base stacking couplings. Although 2D IR spectrometers are not yet widely available, the coupling model tested here is not limited to interpreting 2D IR studies. Rather, it can be used to better interpret and predict the FTIR spectra in DNA/RNA structural and kinetic studies.

Materials and Methods

Sample Preparation. The double-stranded, self-complimentary sequences 5′-d(GGGGGCCCCC)-3′ (referred to as dG_5C_5) and 5′-d(GCGCGCGCGCGCGCGCG)-3′ (referred to as $d(GC)_8$) were each buffered in D_2O with pD = 6.9 at 500 μM concentrations. The dG_5C_5 and $d(GC)_8$ oligonucleotides have T_m at 46.7 and 67.1 °C, respectively, which is the temperature at which 50% of the sample is single-stranded. Below the melting temperature, the concentration of single-stranded oligomers decreases quadratically as a function of temperature. Thus the sample is ∼98% double-stranded at the temperature of the experiments (21 °C). The oligomers dG_5C_5 and $d(GC)_8$ were synthesized by Integrated DNA Technologies, Inc. The oligomer samples were denatured at 80 °C for 4 min and slow-cooled to room temperature to induce helix formation. The UVCD spectrum of $d(GC)_8$ contains a positive peak at 280 nm, a negative peak at 250 nm of equal intensity, and is zero at 260 nm. These features indicate the $d(GC)_8$ oligomer to be in the B-form. This is also consistent with published NMR and X-ray structures of $d(GC)_3$.[34,35] In contrast, the UVCD spectrum of dG_5C_5 exhibits a positive peak at 260 nm, is zero at 246 nm, and is independent of salt concentrations between 50 mM and 1 M for a 100 μM sample concentration, consistent with A-form DNA. The structure of a similar sequence dG_4C_4 has been solved with X-ray crystallography.[37] It is in the A-form with standard Watson−Crick base pairing. Also reported are the FTIR spectra of cytosine (C) and guanine (G) bases, their thione derivatives, and their deoxymonophosphates (dCMP and dGMP), all of which were purchased from Sigma-Aldrich.

Linear and Nonlinear IR Spectroscopy. All samples were held between two CaF_2 plates with a 25-μm-thick spacer. The optical densities of the samples ranged from 0.05 to 0.10. The FTIR spectra were collected at ambient temperatures (21 °C) by using a Mattson Galaxy series FTIR 7000.

In third-order pulsed 2D IR spectroscopy, three infrared femtosecond pulses are used to generate a time-evolving polarization that radiates an electromagnetic field. The bandwidths of the pulses span the vibrational modes of interest, which in this case is 122 cm^{-1} fwhm with a center frequency of 1664 cm^{-1} (they are $<1.1x$ transform limited). The three pulses entered the sample from three different directions (wave vectors) k_1, k_2, and k_3. We monitored the signal field that is emitted in the $k_s = -k_1 + k_2 + k_3$ phase matching direction. The time evolution of the signal field is measured with a local oscillator beam that heterodynes the emitted field in a balanced heterodyne detection configuration by using two mercury cadmium telluride (MCT) detectors. The four pulses are separated in time by the delays t_1, t_2, and t_3, and each of the four pulses has a polarization denoted as (p_1, p_2, p_3, p_{LO}). The 2D IR spectra are generated by double Fourier transforming time-domain data sets collected by stepping along t_1 and t_3 with $t_2 = 0$, which created the $-\omega_1$ and ω_3 axes of the spectra. Time delays are set with computer-controlled translation stages that translate wedged ZnSe optics, altering the time delays through increased material in the infrared path length. The delay lines have a resolution of 0.01 fs, have an absolute accuracy of 0.32 fs, and produce 2D IR spectra that are calibrated to 1.3 cm^{-1}. The pulse widths broaden <1 fs and the phase rotates by $<6.0 \times 10^{-4}$ radians by the change in thickness of ZnSe over the pulse delay.[61] The chosen pulse orderings and phase matching direction selects for a photon echo pulse sequence that enhances the frequency resolution of the spectra by line-narrowing the peaks.[19] Only absolute value 2D IR spectra are reported. Although not reported here, the real parts of the (0°, 0°, 0°, 0°) and (0°, 90°, 90°, 0°) 2D IR spectra were phased relative to one another by matching the positive and negative features of the diagonal peaks. This phasing allowed us to check for sign reversal of the cross-peaks, a measure of the transition dipole relative angle.[19] More detailed descriptions for generating and interpreting 2D IR spectra have been given elsewhere.[20,31]

Computational Methods. All geometry optimizations and frequency calculations were performed by using density functional theory (DFT), employing the hybrid functional B3LYP and the 6-31++G** basis set (denoted DFT throughout this article). Full geometry optimizations and frequency calculations were done on the bases, the thione derivatives, and a G:C base pair. The normal coordinates for C and G that contain the most carbonyl stretch character are denoted Q_C and Q_G, respectively. Single point energy (SPE) calculations were done after perturbing the bases $\pm 0.03 * Q_n$ from equilibrium. The SPE calculations were performed using the DFT method described above, as well as by an ab initio method using the MP2 perturbation theory and the 6-311+G** basis set (denoted MP2 throughout this article). All of these calculations were carried out in Gaussian 98 and Gaussian 03.[38,39] Because all atoms in the mode were perturbed $\pm 0.03 * Q_n$ according to the displacements given in the frequency calculations, partial geometry optimizations were not necessary. The results of the SPE calculations were used in the finite differentiation method to calculate coupling constants and transition dipoles in the base pair and double-stranded DNA (dsDNA) models.

Results

Linear and 2D IR Spectra of dG_5C_5 and $d(GC)_8$. The $d(GC)_8$ oligomer has alternating guanine and cytosine bases along each strand and adopts a B-form secondary structure with standard Watson−Crick base pairing under the conditions used in this study.[34] The linear and absolute value 2D IR spectra of $d(GC)_8$ are shown in Figure 2a−d. Four peaks are observed in the linear spectrum, labeled A−D in Figure 2a, and each of these peaks creates a diagonal peak in the 2D IR spectra of Figure 2b. The "diagonal" peaks are actually composed of anharmonically shifted doublets that are not resolved in the absolute value spectra shown here, but are the reason that peaks A−D do not lie exactly on the diagonal. Peak A has traditionally been assigned to the cytosine ring mode, peaks B and C to

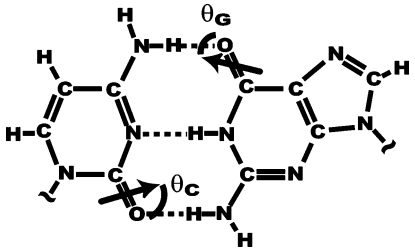

Figure 1. Hydrogen-bonded G:C basepair. The transition dipole vectors are set at the midpoint of the carbonyl bonds and rotated by θ_G and θ_C.

cytosine carbonyl modes, and peak D to the guanine carbonyl mode.[1−3,10,12,40,41] Although we will refer to these modes by their traditional assignments, a major aim of this paper is to determine the actual vibrational motions that underlie these bands. The guanine frequency in $d(GC)_8$ is 19 cm^{-1} higher than that of the dGMP monophosphate base, whereas the cytosine has the same frequency as the base in dCMP. Peaks E−H are cross-peaks between the carbonyl stretch modes and indicate that the G and C bases are coupled. While peaks B and C are not well resolved in the linear spectrum, each creates a cross-peak in the 2D IR spectra, creating doublets that appear above (peaks E and F) and below (peaks G and H) the diagonal. In this work, we quantify and elucidate the origins of the carbonyl−carbonyl coupling interactions that give rise to the observed frequency shifts and cross-peaks.

The spectrum in Figure 2b was acquired using four femtosecond infrared pulses with identical polarizations, e.g., oriented (0°, 0°, 0°, 0°) with respect to the laboratory frame. The spectrum in Figure 2c was collected using the polarization condition (0°, 90°, 90°, 0°), where two of the four pulses were polarized perpendicular to the other two. The large intensity changes in the spectra between (0°, 0°, 0°, 0°) and (0°, 90°, 90°, 0°) indicate that the relative angle between the transition dipoles at peaks B and C are roughly orthogonal.[19] The phases of the cross-peaks in the real parts of the (0°, 0°, 0°, 0°) and (0°, 90°, 90°, 0°) 2D IR spectra also invert, which is consistent with an angle >45° (not shown). The spectrum in Figure 2d was acquired using the polarizations (45°, −45°, 90°, 0°), which reduces the contribution of the diagonal peaks to the spectrum, enhancing the contribution of the cross-peaks.[42] It is clear from the (45°, −45°, 90°, 0°) spectrum that the carbonyl vibrational modes are strongly coupled. The fact that there still remains some intensity near peak D in the (45°,-45°, 90°, 0°) spectrum indicates that there are unresolved cross-peaks hidden beneath the guanosine diagonal peak. The origin of these cross-peaks becomes clearer in the simulations that follow.

The dG_5C_5 model oligomer forms an A-form double-stranded helix that is similar to poly(dG)−poly(dC) under the conditions used in this study.[37,43] Like $d(GC)_8$, the FTIR spectrum of dG_5C_5 also has features that correspond to cytosine ring mode, cytosine carbonyl stretch, and guanine carbonyl stretch modes. However, dG_5C_5 only exhibits a single cytosine carbonyl stretch band rather than two, and as a result, there is only a single cross-peak above and below the diagonal (peaks D and E) rather than the two doublets in $d(GC)_8$. Reproduced from our earlier publication,[44] the polarized 2D IR spectra of dG_5C_5 in Figure 3b−d are also markedly different than that for $d(GC)_8$. Because both strands form Watson−Crick base pairs, this observation indicates that the infrared spectra of DNA cannot be interpreted solely based on the coupling between hydrogen-bonded bases, but that coupling among stacked bases must be important as well.

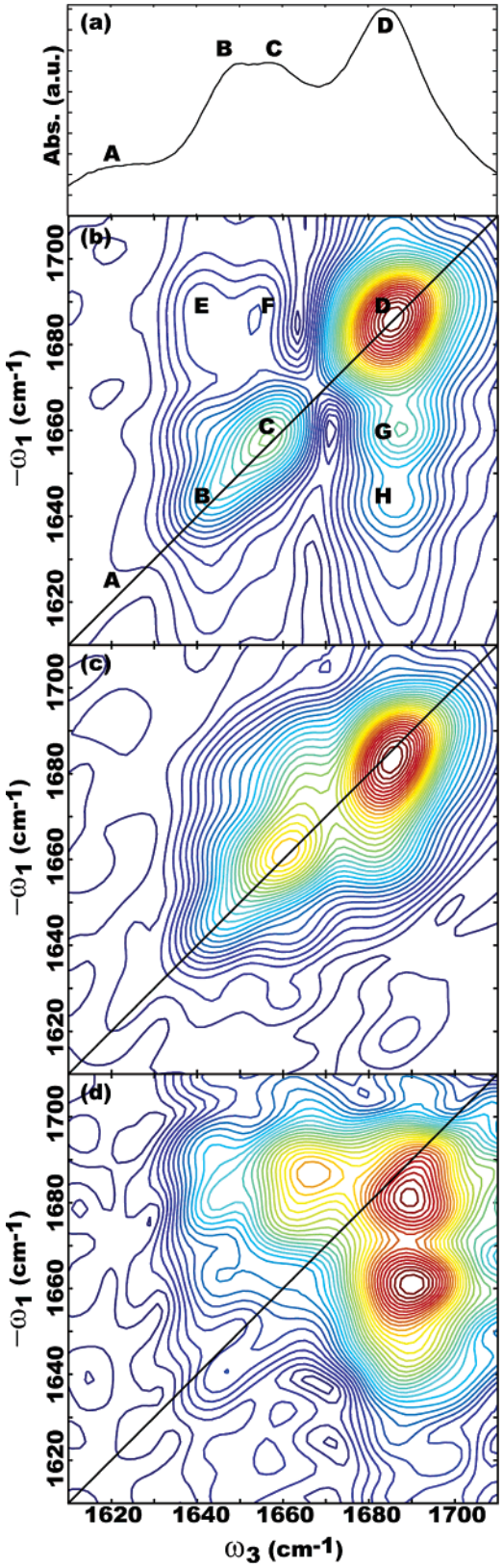

Figure 2. Linear and 2D IR spectra of $d(GC)_8$. (a) Linear-IR spectrum. (b) (0°, 0°, 0°, 0°) 2D IR spectrum. (c) (0°, 90°, 90°, 0°) 2D IR spectrum. (d) (45°, −45°, 90°, 0°) 2D IR spectrum.

Calculated Coupling Constants and Vibrational Spectra. Of central interest to this study is the physical origin of the coupling that gives rise to the FTIR and 2D IR spectra of DNA. In principle, the vibrational frequencies and anharmonicities of the observed eigenstates can be calculated for any molecule or structure from ab initio or density functional methods, but in

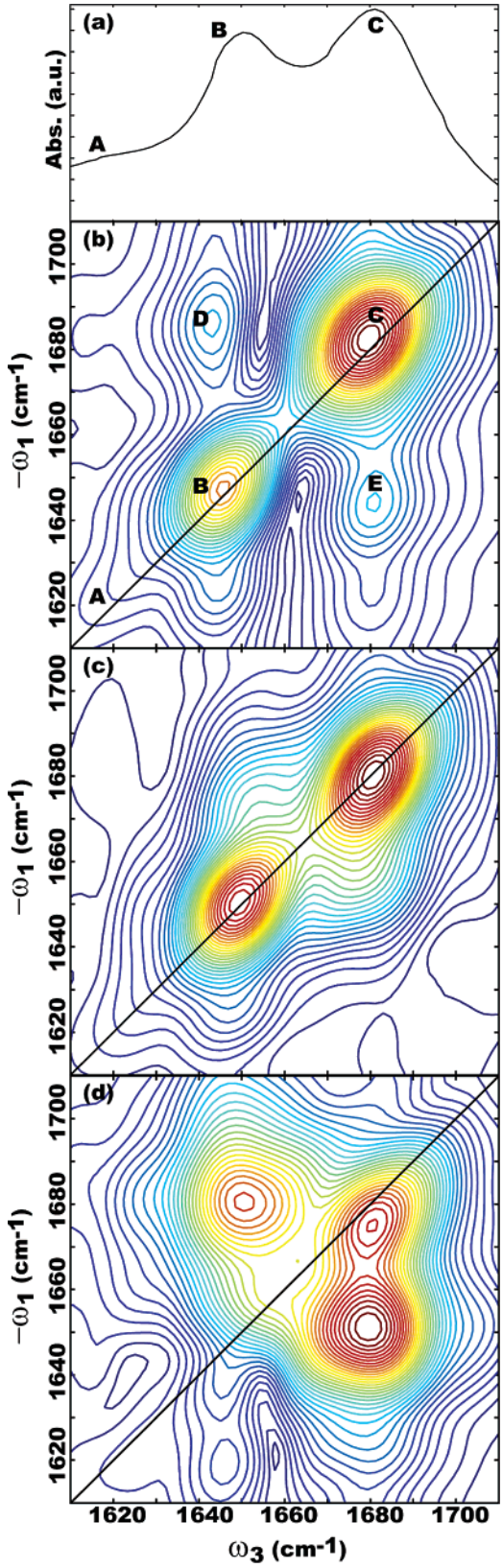

Figure 3. Linear and 2D IR spectra of dG_5C_5. (a) Linear-IR spectrum. (b) (0°, 0°, 0°, 0°) 2D IR spectrum. (c) (0°, 90°, 90°, 0°) 2D IR spectrum. (d) (45°, −45°, 90°, 0°) 2D IR spectrum.

practice, the calculations are too expensive for oligomers of more than a few bases. As a result, it is necessary to develop coupling models that can predict the observed frequencies and anharmonicities for a given oligomer sequence and structure. A coupling model also has the added benefit of providing physical insight into the origins of the coupling so that the spectra can be interpreted intuitively. To this end, we write the vibrational Hamiltonian as

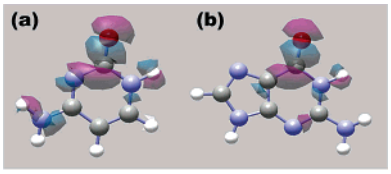

Figure 4. Transition densities of cytosine (a) and guanine (b) plotted at a contour level of 0.001 esu/bohr.

$$H = \frac{1}{2}\sum_i \omega_i B_i^+ B_i - \sum_i \left(\frac{\Delta_{ii}}{2}\right)(B_i^+)^2 B_i^2 + \sum_{i,j} \beta_{ij} B_i^+ B_j \quad (1)$$

where, B_i and B_i^+ are the harmonic oscillator raising and lowering operators, ω_i is the mode frequency, Δ_{ii} is the diagonal anharmonicity of that mode, and β_{ij} are the couplings between these modes.[45] The raising and lowering operators operate on modes Q_n that are localized on the bases. In our analysis that follows, Q_n are the normal modes of the cytosine and guanine bases that contain the most carbonyl stretch motion, as determined by gas-phase frequency calculations. These "local modes" serve as the basis set used to calculate the couplings and simulate the 2D IR spectra. β_{ij} couples these Q_n to create excitonic vibrational modes that extend over multiple bases. β_{ij} is caused by the electron density of one base's mode, Q_n, affecting the nuclear motions of another, Q_m, the origins of which can be electrostatic, electrodynamic, or mechanical. The magnitudes and physical origins of β_{ij} are the main focus of this paper.

The eigenvalues of eq 1 give the frequencies that can be observed in the FTIR and 2D IR spectra. To obtain the intensities of the observable frequencies, we assign a transition dipole μ_n to each mode Q_n and use the eigenvectors of eq 1 to make linear combinations of μ_n. In this study, we locate the transition dipoles at the middle of the carbonyl bonds in the bases at an orientation θ_n (see Figure 1). The resulting eigenstate frequencies and transition dipoles are then used in a perturbative description of infrared spectroscopy to generate stick spectra, which give the FTIR and 2D IR spectra when convoluted with a 1D or 2D line shape function, respectively. Our approach is similar to many studies on peptides[22,45] and we used a similar approach in our initial publication on DNA.[44]

Figure 4 shows plots of the transition density for Q_n on the cytosine and guanine bases. These density plots are created by subtracting the electron density of the isolated bases displaced $\pm 0.03 * Q_n$. The majority of the transition dipole density resides on the carbonyl bonds, but there is significant density distributed throughout the entire ring system because many of the atoms contribute to the motion of these vibrational modes. Thus, these modes cannot be classified as solely carbonyl stretch modes, as other calculations have pointed out as well.[41,46−48] DFT calculations on guanine and cytosine predict transition dipole vectors with oscillator strengths of $\mu_G = 4.25$ D/Å*amu$^{1/2}$ and $\mu_C = 4.19$ D/Å*amu$^{1/2}$, roughly equivalent to experimental values using dCMP and dGMP (3.6 D/Å*amu$^{1/2}$ and 3.9 D/Å*amu$^{1/2}$, respectively). The DFT calculations predict them to be oriented at $\theta_G = 8.63°$ and $\theta_C = 0.20°$ relative to the guanine and cytosine carbonyl bond axes, respectively.

The simplest coupling model that might be applied to DNA bases is transition dipole−dipole coupling. Transition dipole coupling (TDC)[49] is an electrostatic model and is given by

$$\beta_{ij} = \frac{1}{4\pi\epsilon_o} \frac{|\mu_i||\mu_j| - 3(\mu_i \cdot \hat{n})(\mu_j \cdot \hat{n})}{R_{ij}^3} \quad (2)$$

In the TDC coupling calculations reported below, the transition dipoles were located at the midpoint of the carbonyl bonds and oriented along the bond axis. Their magnitudes were set as $\mu_G = \mu_C = 3.8$ D/Å*amu$^{1/2}$. Transition dipole coupling has received widespread use in interpreting the linear and 2D IR spectroscopy of the amide I bands in peptides.[45,49−51] It is a reasonable approximation when the vibrational modes are well separated in space and not covalently bonded, but it fails for modes that are closely spaced. Closely spaced modes require higher-order expansions of the electrostatic potential. In cases where this occurs, multiple charge[52] or transition dipole density[16] models may be better. The transition dipole density distribution (TDDD) model calculates the coupling according to

$$\beta_{ij} = \sum_{n,m} \frac{M_{in}^A M_{jm}^B}{R_{nm}} \quad (3)$$

where

$$M_{in}^A(\vec{r}_n) = \delta V_n \int_{\vec{r}_n}^{\vec{r}_n + \delta\vec{r}_n} d\vec{r}_n \left(\frac{\delta\rho(\vec{r}_n)}{\delta Q_i}\right)_0 \quad (4)$$

In eq 4, the transition density (Figure 4) is given by ρ at a collection of grid points, n, summed over nonoverlapping volumes A and B. The TDDD model is a more accurate representation of electrostatic coupling than the TDC model and approximates the coupling in β-sheet peptides quite well.[16] The TDDD coupling values given below were calculated using transition dipole densities that were generated during SPE calculations using the DFT method described above.

In cases where there is charge flow, the electrostatic models break down and more sophisticated models are required such as finite difference and Hessian reconstruction methods.[50,53] The finite difference method relies on the fact that the coupling constants β_{ij} are related to the curvature of the potential with respect to the local modes Q_i and Q_j and, therefore, can be obtained by analytical differentiation of the potential along the two modes,

$$\beta_{ij} = \frac{\partial^2 E(Q_i, Q_j)}{\partial Q_i \partial Q_j} \quad (5)$$

By generating the potential from electronic structure calculations, the coupling includes both electrostatic and dynamic charge effects.

Vibrational Coupling between Hydrogen-Bonded G and C Bases. Central to predicting the IR spectra of DNA and RNA is the understanding of the vibrational coupling between bases in Watson−Crick base pairs, which has been the focus of many other studies.[10,48,54] Guanine and cytosine are connected by three hydrogen bonds in a Watson−Crick base pair. Electrostatic, electrodynamic, and mechanical effects could potentially contribute to the coupling in hydrogen-bonded bases. The hydrogen bonds might also mechanically couple the motions of the carbonyl and ND_2 modes. Certainly, electrostatic coupling will be significant because the carbonyl groups have large transition densities (Figure 4) and are located in close proximity to one another (4.9 Å).

Table 1 lists the coupling strengths calculated between the hydrogen-bonded G and C bases in a Watson−Crick base pair using the three methods outlined above, e.g., TDC, TDDD, and finite difference methods. All three models predict significant negative coupling between hydrogen-bonded bases but differ in magnitude. The finite difference method, which accounts for mechanical, electrostatic, and electrodynamics effects, gives $\beta_{GC} = -12$ cm^{-1} whether calculated with our DFT or MP2 methods. In comparison, the TDDD method, which is purely an electrostatic model, predicts a comparable strength of -13 cm^{-1}. The electrostatic TDC model predicts only -5.5 cm^{-1} of coupling. To test for electrodynamic effects, we calculated the transition density for each base in the presence of the complimentary base held at equilibrium. The results (not shown) were compared to Figure 4. No appreciable transition density resides on the base held at equilibrium, indicating that electrodynamic effects are minor.[16] Thus, we conclude from these calculations that the coupling mechanism between hydrogen-bonded G and C bases in Watson−Crick base pairs is primarily electrostatic in nature. Comparison to experiments discussed below suggest that the coupling between hydrogen-bonded G:C base pairs can be calculated quite reliably by using the TDDD and finite difference methods but is underestimated with TDC.

TABLE 1: Calculated Coupling Strengths in the Hydrogen-Bonded G:C Basepair

method	β_{ij} (cm^{-1})
TDC	−5.5
TDDD	−13.8
finite difference DFT	−12.9
finite diff erence MP2	−11.6

Vibrational Coupling between Nearest-Neighbor Bases. The secondary structures of dG_5C_5 and $d(GC)_8$ can be broken into repeating segments of stacked Watson−Crick base pairs, as shown in Figures 5 and 6. In Figure 5, the repeating unit for dG_5C_5 is shown. It consists of two G:C base pairs oriented in A-form geometry. In Figure 6, the repeating segment in $d(GC)_n$ is shown that consists of two units, A and B. Unit A is a G:C base pair on top of a C:G base pair. Unit B is a C:G base pair stacked on top of a G:C base pair. These two units are not equivalent because of the DNA helicity. The structure of $d(GC)_n$ contains n of unit A and $n-1$ of unit B stacked in an alternating fashion.

In the limit that the coupling between bases separated by more than one base pair is negligible, the repeating patterns also give the minimum number of coupling parameters necessary to model the vibrational Hamiltonian. These coupling parameters are shown schematically in Figures 5 and 6. Truncating the vibrational Hamiltonian to nearest neighbors is probably a reasonable approximation considering that the coupling between bases scales with distance as R^{-3}, at least according to transition dipole coupling. We have tested this approximation for d(GGG) in A-form, which has the largest coupling between any combination of bases studied here. According to TDC and the finite difference method with DFT calculations, the coupling between two stacked guanines in d(GGG) is $\beta_G \approx 19$ cm^{-1} (Table 2), whereas the coupling between first and third guanines is $\beta_{G2} \approx 2$ cm^{-1}. As discussed below, neither of these models predicts the correct absolute coupling between stacked guanines, but we expect that the relative trend will hold.

The coupling constants for repeating segments of dG_5C_5 and $d(GC)_8$ are listed in Tables 2 and 3, respectively. These terms were computed using transition dipole coupling, and finite difference with DFT or MP2. For most coupling terms, all three methods predict the same signs, although the magnitudes of the TDC couplings typically disagree with the finite difference methods by 2−5 cm^{-1}. DFT and MP2 calculations agree to

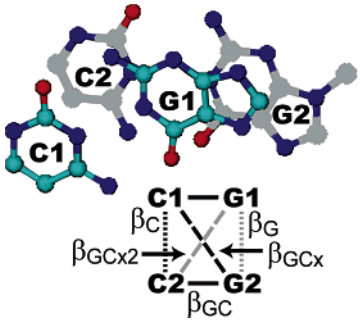

Figure 5. Coupling model for dG_nC_n.

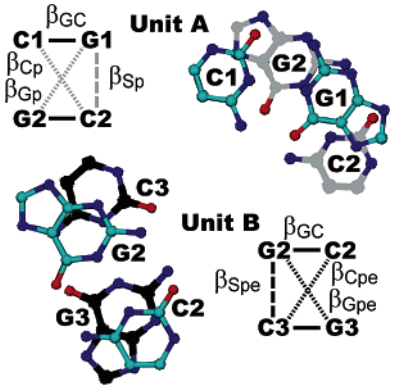

Figure 6. Coupling model for $d(GC)_n$.

TABLE 2: Calculated and Experimental Best-Fit Coupling Parameters for DG_5C_5

coupling term	sites	TDC (cm^{-1})	B3LYP (cm^{-1})	MP2 (cm^{-1})	experimental best-fit (± 2 cm^{-1})
β_{GC}	G1, C1	−5.5	−10.4	−11.6	−9.6
β_G	G1, G2	18.7	21.8	12.6	9.5
β_C	C1, C2	0.6	1.0	−0.45	0.7
β_{GC_x}	C1, G2	−2.05	−1.6	−3.0	−1.9
β_{GC_x2}	G1, C2	−2.35	−5.0	−4.7	−2.7

TABLE 3: Calculated and Experimental Best-fit Coupling Parameters for $D(GC)_8$

coupling term	sites	TDC (cm^{-1})	B3LYP (cm^{-1})	MP2 (cm^{-1})	experimental best-fit (± 2 cm^{-1})
		Unit A			
β_{GC}	G1, C1	−5.5	−10.4	−11.6	−10.6
β_{Sp}	G1, C2	−5.6	−9.6	−9.4	−5.32
β_{Gp}	G1, G2	11.4	8.2	8.0	8.2
β_{Cp}	C1, C2	1.6	1.2	1.6	2.15
		Unit B			
β_{GC}	G2, C2	−5.5	−10.4	−11.6	−10.6
β_{Spe}	G2, C3	4.2	3.0	1.1	0.5
β_{Gpe}	G2, G3	2.2	6.7	6.7	2.9
β_{Cpe}	C2, C3	4.6	3.3	4.4	2.8

within 1−2 cm^{-1} for all coupling constants except between stacked guanines, β_G, in dG_5C_5. DFT probably fails for β_G because the London dispersion forces are not predicted correctly by the exchange-correlation functional. London dispersion forces are induced dipole−induced dipole interactions that are responsible for stabilizing DNA stacking interactions and are proportional to R^{-6}. It has been reported that the exchange-correlation functionals used in B3LYP do not have the proper R^{-6} dependence and thus predict repulsive interactions when they should be attractive.[55−57] Of all the combinations of stacked bases, the rings of stacked guanine bases in the A-form have the most overlap, as can be seen in Figures 5 and 6, leading to

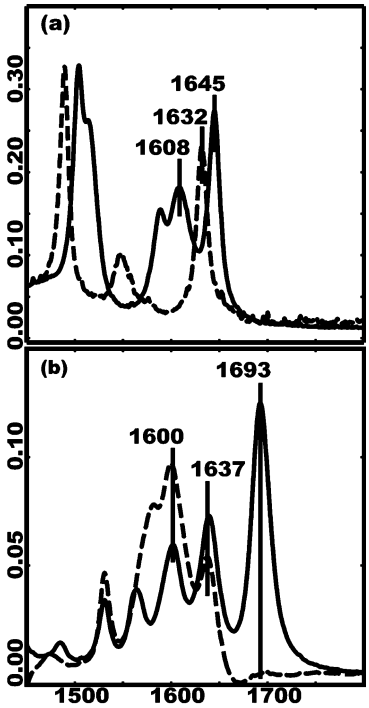

Figure 7. Linear-IR spectra of (a) cytosine (solid) and 2-thiocytosine (dashed) in D_2O and (b) guanine (solid) and 6-thioguanine (dashed) in DMSO.

TABLE 4: Experimental and Calculated Frequencies for Cytosine, Guanine, and Their Thione Derivatives

molecule	dominate coordinate	calcd frequency (cm^{-1})	obsd frequency (cm^{-1})
cytosine	C═O stretch	1785	1645
	ring, C═C stretch	1711	1608
2-thiocytosine	C═S stretch	1185	650
	ring, C═C stretch	1708	1632
guanine	C═O stretch	1840	1693
	ring, C═N stretch	1646	1637, 1600
6-thioguanine	C═S stretch	1000	650
	ring, C═N stretch	1649	1637, 1600

the largest failure of the DFT B3LYP calculations. Another method that failed was TDDD (eqs 3 and 4). We calculated many of the coupling constants using TDDD, but we do not report them because this model did not give physically meaningful values for stacked systems. It is possible that TDDD fails because of charge transfer along the DNA strands, which is discussed below.

Refinement of the Normal Modes. In the next section, we present experimental evidence that the above computational methods are good predictors of DNA vibrational couplings. However, we also have experimental evidence that the normal modes of cytosine are not correctly predicted by density functional theory. Shown in Figure 7a are the FTIR spectra for cytosine (solid) and 2-thiocytosine (dashed), which has the carbonyl oxygen replaced by a sulfur atom. According to DFT calculations given in Table 4, the experimental cytosine peak at 1645 cm^{-1} is the mode that has predominately carbonyl stretch character and whose transition density is shown in Figure 4. This band is predicted to have 4.5 times more carbonyl displacement than ring C═C bond displacement. In contrast, the peak at 1608 cm^{-1} is assigned the ring C═C bond stretch because its displacement is nine times larger than the carbonyl displacement. These displacements suggest that the ring C═C and C═O modes are decoupled, which was computationally confirmed by also calculating the ring C═C and C═S modes

of 2-thiocytosine given in Table 4. In the 2-thiocytosine calculations, the C═S stretch appears at ~1185 cm^{-1}, effectively removing this local mode from the measured frequency range. The fact that the frequency of the ring C═C stretch only shifts 3 cm^{-1} upon sulfur substitution (from 1711 to 1708 cm^{-1}) in the DFT calculations indicates that the two modes are only weakly coupled. However, these assignments are inconsistent with the experimental FTIR spectrum of 2-thiocytosine. Experimentally, the ring C═C mode of 2-thiocytosine shifts up 24 cm^{-1} to 1632 cm^{-1} and lies approximately halfway between the original two bands at 1608 and 1645 cm^{-1}. So, rather than being decoupled, the FTIR spectra suggest that the carbonyl and ring C═C stretch modes in cytosine have nearly degenerate frequencies that are coupled by ~24 cm^{-1}. A different situation arises for guanine. Like cytosine, DFT calculations on guanine and 6-thioguanine predict that the ring C═N and C═O modes are uncoupled. But unlike cytosine, this assignment is experimentally confirmed by the FTIR spectra of guanine and 6-thioguanine (Figure 7b), which both have the same ring C═N stretch frequency. Thus, we conclude that the DFT calculations correctly predict the character of the C═O and ring C═N modes in guanine, but that, in cytosine, the modes at 1608 and 1645 cm^{-1} really correspond to very strongly coupled carbonyl and ring C═C vibrations that form symmetric and antisymmetric stretches.

Underestimating the amount of ring C═C stretch that is in the "carbonyl" stretch of cytosine has two potential ramifications to our study. First, the ring C═C stretch may contribute to the couplings. Using finite difference, we recalculated β_{GC} and β_{Sp} with the carbonyl stretch frozen and the amplitude of the ring C═C stretch mode scaled upward by a factor of 4 to match the carbonyl amplitude. The recalculated couplings fell within 2 cm^{-1} of their original values. β_{Sp} was chosen because the distance between the cytosine ring C═C stretch and the guanine carbonyl stretch is the smallest of all base combinations. Therefore, we conclude that underestimating the ring C═C stretch contribution has at most a 1.5 cm^{-1} effect on the coupling values listed in Tables 2 and 3 because it is the carbonyl stretch that is largely responsible for the coupling magnitudes. Second, underestimating the ring C═C motion means that the transition dipole direction of cytosine calculated with DFT is inaccurate. The transition dipole vector of the ring mode in 2-thiocytosine has an oscillator strength of 3.88 D/Å*$amu^{1/2}$ that is nearly equivalent to the transition dipole of the carbonyl stretch 4.19 D/Å*$amu^{1/2}$. Furthermore, the ring mode transition dipole is orientated 40.0° to the carbonyl transition dipole. Therefore, the transition dipole of the antisymmetric stretch that is probed in our experiment lies somewhere between, perhaps at −71° if the ring C═C and C═O modes contribute equally and have the oscillator strengths mentioned above (approximated by vector summation). The peak intensities in 2D IR spectra are very sensitive to the relative orientations of coupled transition dipoles, which can be used to constrain the cytosine transition dipole direction. In the simulations that follow, we restrict the guanine transition dipole to be within 10° of the guanine carbonyl bond during our fits, as predicted by our DFT and MP2 calculations, and rotate the cytosine transition angle for best agreement with experiment.

Simulated IR Spectra of dG_5C_5 and $d(GC)_8$. By using the coupling constants listed in Table 3 as a guide, we simulated the 2D IR spectra of $d(GC)_8$, following eq 1 and the procedure outlined above. The best-fit linear and 2D IR spectra of $d(GC)_8$ are shown in Figure 8a−d. The peak frequencies, intensities, and polarization dependence are all closely reproduced, indicating that the simulated eigenstates have the proper transition strengths and directions. Table 5 lists the mode frequencies ω_i, the diagonal anharmonicities Δ_{ii}, transition dipole magnitudes μ_n, and angles θ_n used in the simulations. The Δ_{ii} parameters were measured with pump−probe studies on the monophosphate

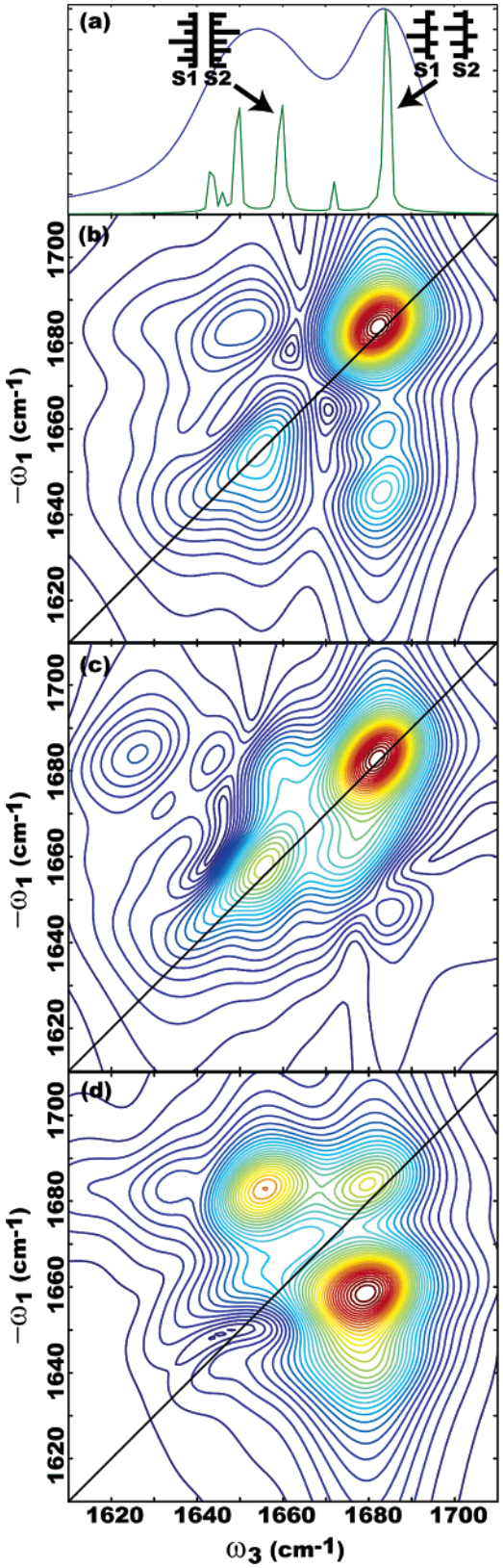

Figure 8. Simulated linear and 2D IR spectra of $d(GC)_8$. Polarizations in b−d match those in Figure 2.

TABLE 5: Local Mode and Lineshape Parameters Used in Simulated IR Spectra of dG_5C_5 and $d(GC)_8$

parameter	dG_5C_5	$d(GC)_8$
ω_G (cm^{-1})	1664.0	1666.2
ω_C (cm^{-1})	1655.6	1652.0
θ_G (deg)	−1.0	−2.1
θ_C (deg)	−87.9	−67.3
Δ_G (cm^{-1})	14.0	14.0
Δ_C (cm^{-1})	9.0	9.0
μ_G D/A*amu$^{1/2}$	3.8	3.8
μ_C D/A*amu$^{1/2}$	3.8	3.8
γ (cm^{-1})	6.6	8.4
σ (cm^{-1})	4.4	5.4

bases and were not varied in the experiment.[44] The ω_i were constrained to be within 4 cm^{-1} of their monophosphate frequencies in D_2O. The 2D line shapes were generated by Fourier transforming the nonlinear response for a single oscillator in the Bloch limit by using the homogeneous (γ) and inhomogeneous (σ) parameters in Table 5. Table 3 lists the best-fit coupling parameters for comparison to the calculated values. The fits are quite sensitive to the parameters because the calculated eigenstates must reproduce the pair of cross-peaks and the polarization dependence of the spectra, but the error in the coupling parameters is hard to quantify because it is mostly systematic. We assign error bars of ±2 cm^{-1} to the coupling parameters, estimated by varying each coupling constant and compensating with the other parameters until the spectra are no longer adequately fit. Although the spectra are more sensitive to some coupling terms than others, these error bars conservatively encompass the deviations associated with the least-sensitive parameters. We also found that, because A- and B-form have different helical tilts, it was impossible to satisfactorily fit the 2D IR spectra using the wrong helical form; $d(GC)_8$ could not be modeled with A-form, and dG_5C_5, discussed below, could not be modeled with B-form no matter how the coupling constants were varied. This phenomenon occurs because the helical tilt changes the relative orientations of the transition dipoles that in turn alter the intensities and polarization dependence of the peaks in the 2D IR spectrum.

Fits to the 2D IR spectra of dG_5C_5 are shown in Figure 9a–d. The best-fit parameters are given in Tables 2 and 5. Like $d(GC)_8$, the 2D IR spectra of dG_5C_5 reproduce the experimental spectra remarkably well. Moreover, the local mode parameters listed in Table 5 are very similar for the two strands, consistent with both strands being composed of Watson–Crick base pairs.

Discussion

Coupling Hamiltonians in the spirit of eq 1 have been proposed in earlier work and used to interpret FTIR and VCD spectra.[10–12,40] One such study used FTIR isotope labeling studies on poly(dG)–poly(dC) and concluded that the G and C carbonyl modes are coupled by $\beta_{GC} = 15.3$ cm^{-1},[10] 50% more than the coupling we find by experiment and theory in this report for dG_5C_5, our equivalent strand to poly(dG)–poly(dC). However, the FTIR isotope labeling study neglected coupling between stacked bases. In a separate VCD study on $d(GC)_4$, the coupling between stacked guanine and cytosine bases was found to be ~35 cm^{-1},[11] more than 30 cm^{-1} larger than our experiments or calculations predict for $d(GC)_8$ (coupling terms β_{Sp} and β_{Spe}). The VCD simulations neglected base pair coupling. Thus, neither study used a complete Hamiltonian with both base pairing and base stacking couplings. From our studies reported here, we know that both base pairing and base stacking couplings are important, but without an established coupling model, approximations to the Hamiltonian are necessary in order to interpret these linear spectra because they do not provide enough observables for a unique determination of both coupling types. In principle, one could ascertain the complete vibrational coupling Hamiltonian in eq 1 with sufficient isotope labeling studies, but in practice, this is not feasible. With 2D IR spectroscopy, many more observables are generated, including the frequencies of the overtone and combination bands (which

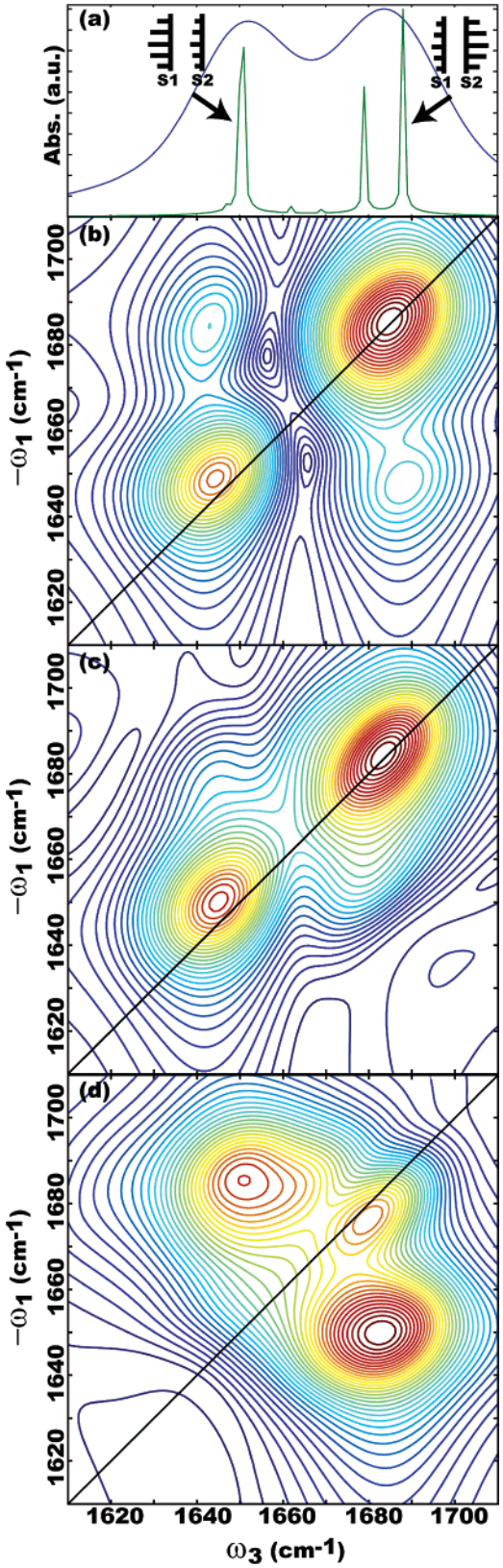

Figure 9. Simulated linear and 2D IR spectra of dG_5C_5. Polarizations in b–d match those in Figure 3.

are the origins of the cross-peaks) and peak intensities that depend on relative transition dipole angles. Thus, 2D IR spectroscopy provides a much more comprehensive test of vibrational coupling models.

With the spectra fit and the coupling constants determined, we can now understand the characteristic frequency shifts that occur upon duplex formation of these two strands. Consider dG_5C_5: upon duplex formation, the guanosine frequency shifts up 19 cm^{-1} from the base frequency to 1684 cm^{-1} while the cytosine frequency remains nearly unchanged at 1650 cm^{-1}. The guanosine shift is caused primarily by two coupling interactions that reinforce one another, β_G and β_{GC}. β_G is the coupling between stacked guanine bases (Figure 5) and equals $+9.5$ cm^{-1}. This large and positive coupling term links the stacked guanine bases in dG_5C_5 to make a chain of coupled oscillators, similar to the classic solid-state physics problem of a lattice of coupled oscillators. In fact, the solution to this classic problem predicts that, if this were an infinitely long helix, then the shift is equal to the sum of the stack couplings.[58] Thus, the β_G coupling term alone would produce a guanine frequency shift of 9.5 cm^{-1} (which our coupling Hamiltonian confirms). The second coupling term is $\beta_{GC} = -9.6$ cm^{-1}. This term couples the guanine and cytosine bases to one another, increasing their splitting and shifting the guanine to even higher frequencies. Conversely, this coupling term shifts cytosine to a lower frequency and counteracts the cytosine stack coupling, $\beta_c = +0.7$ cm^{-1}, which is why the cytosine band shifts very little upon duplex formation. Similar qualitative comparisons of the couplings can be made to understand $d(GC)_8$, the main difference being that the stacked bases alternate between guanosine and cytosine, giving alternating stacked couplings that create the splitting in the cytosine peak and the observed doublet cross-peaks in Figure 2.

The vibrational motions that create the observed FTIR spectra are better visualized through the coefficients of the eigenstates of the diagonalized Hamiltonian. In Figure 9a, the eigenvector coefficients are graphed for two of the infrared peaks in dG_5C_5. The two vertical lines represent the cytosine (S1) and guanine (S2) oligomers in dG_5C_5, and each bar gives the magnitude and sign of the coefficient for that base. As is seen in these plots, the G and C bases stretch in unison along the lengths of the strands. The only significant difference between these two eigenstate modes is that the C strand is in phase with the G strand for the lower frequency mode and out of phase with the G strand in the higher mode, creating symmetric and antisymmetric strand stretches. A slightly different situation arises in $d(GC)_8$, shown in Figure 8a. For this helix, the G and C bases still vibrate in unison, but to stay in phase, the cytosine carbonyls on S1 stretches while the cytosine carbonyls on S2 compress because the bonds are antiparallel. The situation is likewise for G. Most previous studies have interpreted the infrared spectra of helical DNA in terms of base pair normal modes.[10,54] However, we find in this study that, even though the coupling between bases in G:C base pairs is strong ($\beta_{GC} = -9.6$ to -10.6 cm^{-1}), the coupling between stacked bases is comparable. For example, the coupling between guanines in A- and B-forms are $\beta_G = 9.5$ and $\beta_{Gp} = 8.2$ cm^{-1}, respectively. As a result, it is actually better to visualize the vibrational motions of DNA, not as base pair vibrations, but as vibrational motions delocalized over the helical strands as well. Future work will characterized the delocalization length of the vibrations by including frequency disorder in the calculations.

Tables 2 and 3 compare the experimentally determined coupling parameters with the values computed from TDC and finite difference methods. Compared to experiment, the TDC model predicts almost all of the correct signs but underestimates the base pair coupling, β_{GC}. It also overestimates the coupling between guanines both in A-form (β_G) and in unit A of B-form (β_{Gp}). On the other hand, the finite difference method using DFT gets β_{GC} to within $1-2$ cm^{-1} and does a reasonable job with most other couplings except for β_G. β_G is the only coupling parameter that significantly improves with MP2, probably because treating dispersion forces properly in the calculation becomes important when there is significant overlap of the stacked bases. Of all the combinations of stacked bases studied here, stacked guanines in the A-form have the most overlap.

One reason that transition dipole coupling cannot fully explain DNA couplings is because of electrodynamics effects. Charge transfer is a well-documented characteristic of DNA,[59,60] and we have found evidence for vibrationally mediated charge transfer between stacked bases. For example, an induced transition dipole of 0.49 $D/A*amu^{1/2}$ is created on the lower of two stacked guanine bases in A-form. The effect is smaller for cytosine bases that have less ring overlap, but still significant (0.38 $D/A*amu^{1/2}$). These effects are included in coupling calculations by using the electronic structure finite difference methods, but not in TDC or TDDD. Charge flow may explain why the transition dipole density approach fails for calculating couplings between stacked bases.

The calculations have been performed on gas-phase bases. Including solvent may alter the potentials and improve the agreement with experiment. The simulations might also be improved by including frequency and coupling disorder created from structural and solvent variations. These effects could be investigated by adding a few water molecules to the calculations, but realistic solvation is impractical, especially for a helix. A more practical means of improving the agreement between theoretical prediction and experiment might be to empirically optimize the transition dipole placement and orientations in TDC calculations as has been done for proteins.[50] We also note that our coupling Hamiltonian may not be rigorous for DNA or RNA hydrated in H_2O rather than D_2O. In D_2O, the ND_2 bending motions associated with the base pair hydrogen bonds reside at lower frequencies ($\sim$1400 cm^{-1}). However, NH_2 bends appear near 1680 cm^{-1} and couple very strongly to the carbonyl motions. Thus, the coupling across bases in base pairs may contain significant mechanical contributions in addition to the strong electrostatic coupling. Further investigation is necessary to test the validity of this reasoning.

Conclusions

In this article, we use 2D IR spectroscopy to test a coupling model for the carbonyl stretches of guanine and cytosine DNA sequences. A local mode description for the coupled carbonyl stretches of peptide backbones (amide I mode) has become a very successful model for interpreting the linear and 2D IR spectra of proteins. Following that example, we show that a similar coupling model works well for G/C DNA sequences that use a basis of vibrational modes localized on individual bases. Most of the coupling terms between the bases can be reliably calculated with finite difference methods employing the DFT computational approaches. While promising, effects such as hydration and charge transfer need to be addressed in more detail. The studies also need to be extended to include adenine and thymine bases, but already, this model allows for a quantitative interpretation of DNA infrared spectra that has been lacking in the literature. The experiments and calculations show that 2D IR spectroscopy is much more sensitive to the structural

variations in DNA and RNA than its linear counterpart. Although FTIR and 2D IR spectra cannot currently be inverted to give a structure with models such as this one, potential secondary structures such as canonical DNA forms, structures from the Protein Data Bank, or structures generated from molecular dynamics simulations can be tested against experiment. The utility of 2D IR spectroscopy is its combination of structure, time-resolution, and experimental versatility with regard to sample volume, concentration, and phase. Taken together, the combination promises to make 2D IR spectroscopy an important tool in monitoring DNA in diverse environments as well as probing the submillisecond structural kinetics of DNA.

Acknowledgment. M.T.Z. thanks Min Cho for helpful conversations. This research was supported by the Beckman Foundation and the National Science Foundation no. CHE0350-518. Computational resources were provided to the UW Chemistry Parallel Computing Center though NSF grant no. CHE0091916 and gifts from the Intel Corporation. A.T.K. also thanks the NSF for a graduate K-12 fellowship.

References and Notes

(1) Masamichi, T. *Appl. Spectrosc. Rev.* **1969**, *3*, 45−90.
(2) Taillandier, E.; Liquier, J. *Methods Enzymol.* **1992**, *211*, 307−335.
(3) Liquier, J.; Taillandier, E. In *Infrared Spectroscopy of Biomolecules*; Mantsch, H.; Chapman, D., Eds.; Wiley-Liss, Inc.: New York, 1996; pp 131−158.
(4) Banyay, M.; Sarkar, M. *Biophys. Chem.* **2003**, *104*, 477−488.
(5) Fritzsche, H. *J. Mol. Struct.* **1991**, *242*, 245−261.
(6) Pichler, A.; Rudisser, S.; Winger, R. H.; Liedl, K. R.; Hallbrucker, A.; Mayer, E. *J. Am. Chem. Soc.* **2000**, *122*, 716−717.
(7) Kuimova, M. K.; Cowan, A. J.; Matousek, P.; Parker, A. W.; Sun, X. Z.; Towrie, M.; George, M. W. *Proc. Natl. Acad. Sci. U.S.A.* **2006**, *103*, 2150−2153.
(8) Brockman, J. M.; Frutos, A. G.; Corn, R. M. *J. Am. Chem. Soc.* **1999**, *121*, 8044−8051.
(9) Torii, H.; Tasumi, M. *J. Chem. Phys.* **1992**, *96*, 3379−3387.
(10) Howard, F. B.; Frazier, J.; Miles, H. T. *Proc. Natl. Acad. Sci. U.S.A.* **1969**, *64*, 451−458.
(11) Gulotta, M.; Goss, D. J.; Diem, M. *Biopolymers* **1989**, *28*, 2047−2058.
(12) Zhong, W.; Gulotta, M.; Goss, D. J.; Diem, M. *Biochemistry* **1990**, *29*, 7485−7491.
(13) Zhang, W. M.; Chernyak, V.; Mukamel, S. *J. Chem. Phys.* **1999**, *110*, 5011−5028.
(14) Gnanakaran, S.; Hochstrasser, R. M. *J. Am. Chem. Soc.* **2001**, *123*, 12886−12898.
(15) Scheurer, C.; Piryatinski, A.; Mukamel, S. *J. Am. Chem. Soc.* **2001**, *123*, 3114−3124.
(16) Moran, A.; Mukamel, S. *Proc. Natl. Acad. Sci. U.S.A.* **2004**, *101*, 506−510.
(17) Demirdoven, N.; Cheatum, C. M.; Chung, H. S.; Khalil, M.; Knoester, J.; Tokmakoff, A. *J. Am. Chem. Soc.* **2004**, *126*, 7981−7990.
(18) Golonzka, O.; Khalil, M.; Demirdöven, N.; Tokmakoff, A. *Phys. Rev. Lett.* **2001**, *86*, 2154−2157.
(19) Zanni, M. T.; Gnanakaran, S.; Stenger, J.; Hochstrasser, R. M. *J. Phys. Chem. B* **2001**, *105*, 6520−6535.
(20) Ge, N.-H.; Zanni, M. T.; Hochstrasser, R. M. In *Ultrafast Phenomena XIII*, Miller, R. J. D. Murnane, M. M., Scherer, N. F., Weiner, A. M., Eds.; Springer-Verlag: New York, 2003; pp 592−594.
(21) Ashbury, J. B.; Steinel, T.; Stromberg, C.; Gaffney, K. J.; Piletic, I. R.; Goun, A.; Fayer, M. D. *Chem. Phys. Lett.* **2003**, *374*, 362−371.
(22) Moran, A. M.; Park, S.-M.; Dreyer, J.; Mukamel, S. *J. Chem. Phys.* **2003**, *118*, 3651−3659.
(23) Yeremenko, S.; Pshenichnikov, M. S.; Wiersma, D. A. *Chem. Phys. Lett.* **2003**, *369*, 107−113.
(24) Bredenbeck, J.; Helbing, J.; Hamm, P. *J. Am. Chem. Soc.* **2004**, *126*, 990−991.
(25) Fang, C.; Hochstrasser, R. M. *J. Phys. Chem. B* **2005**, *109*, 18652−18663.
(26) Hahn, S.; Kim, S.-S.; Chewook, L.; Cho, M. *J. Chem. Phys.* **2005**, *123*, 084905/1−084905/10.
(27) Kurochkin, D. V.; Naraharisetty, S. R. G.; Rubtsov, I. V. *J. Phys. Chem. A* **2005**, *109*, 10799−10802.
(28) Larsen, O. F. A.; Bodis, P.; Buma, W. J.; Hannam, J. S.; Leigh, D. A.; Woutersen, S. *Proc. Natl. Acad. Sci. U.S.A.* **2005**, *102*, 13378−13382.
(29) Zheng, J.; Kwak, K.; Asbury, J.; Chen, X.; Piletic, I. R.; Fayer, M. D. *Science* **2005**, *309*, 1338−1343.
(30) Mukherjee, P.; Kass, I.; Arkin, I.; Zanni, M. T. *Proc. Natl. Acad. Sci. U.S.A.* **2006**, *103*, 3528−3533.
(31) Fulmer, E. C.; Mukherjee, P.; Krummel, A. T.; Zanni, M. T. *J. Chem. Phys.* **2004**, *120*, 8067−8078.
(32) Fulmer, E. C.; Ding, F.; Mukherjee, P.; Zanni, M. T. *Phys. Rev. Lett.* **2005**, *94*, 067402/1−067402/4.
(33) Massari, A. M.; Finkelstein, I. J.; McClain, B. L.; Goj, A.; Wen, X.; Bren, K. L.; Loring, R. F.; Fayer, M. D. *J. Am. Chem. Soc.* **2005**, *127*, 14279−14289.
(34) Lam, S. L.; AuYeung, S. C. F. *J. Mol. Biol.* **1997**, *266*, 745−760.
(35) Eisenstein, M.; Shakked, Z. *J. Mol. Biol.* **1995**, *248*, 662−678.
(36) Saenger, W.; Heinemann, U. *FEBS Lett.* **1989**, *257*, 223−227.
(37) Mccall, M.; Brown, T.; Kennard, O. *J. Mol. Biol.* **1985**, *183*, 385−396.
(38) Frisch, M. J.; Trucks, G. W.; Schlegel, H. B.; Scuseria, G. E.; Robb, M. A.; Cheeseman, J. R.; Zakrzewski, V. G.; Montgomery, J. A., Jr.; Stratmann, R. E.; Burant, J. C.; Dapprich, S.; Millam, J. M.; Daniels, A. D.; Kudin, K. N.; Strain, M. C.; Farkas, O.; Tomasi, J.; Barone, V.; Cossi, M.; Cammi, R.; Mennucci, B.; Pomelli, C.; Adamo, C.; Clifford, S.; Ochterski, J.; Petersson, G. A.; Ayala, P. Y.; Cui, Q.; Morokuma, K.; Malick, D. K.; Rabuck, A. D.; Raghavachari, K.; Foresman, J. B.; Cioslowski, J.; Ortiz, J. V.; Stefanov, B. B.; Liu, G.; Liashenko, A.; Piskorz, P.; Komaromi, I.; Gomperts, R.; Martin, R. L.; Fox, D. J.; Keith, T.; Al-Laham, M. A.; Peng, C. Y.; Nanayakkara, A.; Gonzalez, C.; Challacombe, M.; Gill, P. M. W.; Johnson, B. G.; Chen, W.; Wong, M. W.; Andres, J. L.; Head-Gordon, M.; Replogle, E. S.; Pople, J. A. *Gaussian 98*, revision A.7; Gaussian, Inc.: Pittsburgh, PA, 1998.
(39) Frisch, M. J.; Trucks, G. W.; Schlegel, H. B.; Scuseria, G. E.; Robb, M. A.; Cheeseman, J. R.; Montgomery, J. A., Jr.; Vreven, T.; Kudin, K. N.; Burant, J. C.; Millam, J. M.; Iyengar, S. S.; Tomasi, J.; Barone, V.; Mennucci, B.; Cossi, M.; Scalmani, G.; Rega, N.; Petersson, G. A.; Nakatsuji, H.; Hada, M.; Ehara, M.; Toyota, K.; Fukuda, R.; Hasegawa, J.; Ishida, M.; Nakajima, T.; Honda, Y.; Kitao, O.; Nakai, H.; Klene, M.; Li, X.; Knox, J. E.; Hratchian, H. P.; Cross, J. B.; Bakken, V.; Adamo, C.; Jaramillo, J.; Gomperts, R.; Stratmann, R. E.; Yazyev, O.; Austin, A. J.; Cammi, R.; Pomelli, C.; Ochterski, J. W.; Ayala, P. Y.; Morokuma, K.; Voth, G. A.; Salvador, P.; Dannenberg, J. J.; Zakrzewski, V. G.; Dapprich, S.; Daniels, A. D.; Strain, M. C.; Farkas, O.; Malick, D. K.; Rabuck, A. D.; Raghavachari, K.; Foresman, J. B.; Ortiz, J. V.; Cui, Q.; Baboul, A. G.; Clifford, S.; Cioslowski, J.; Stefanov, B. B.; Liu, G.; Liashenko, A.; Piskorz, P.; Komaromi, I.; Martin, R. L.; Fox, D. J.; Keith, T.; Al-Laham, M. A.; Peng, C. Y.; Nanayakkara, A.; Challacombe, M.; Gill, P. M. W.; Johnson, B.; Chen, W.; Wong, M. W.; Gonzalez, C.; Pople, J. A. *Gaussian 03*, revision C.02; Gaussian, Inc.: Wallingford, CT, 2004.
(40) Wang, L.; Keiderling, T. A. *Biochemistry* **1992**, *31*, 10265−10271.
(41) Andrushchenko, V.; Wieser, H.; Bour, P. *J. Phys. Chem. B* **2002**, *106*, 12623−12634.
(42) Zanni, M. T.; Ge, N. H.; Kim, Y. S.; Hochstrasser, R. M. *Proc. Natl. Acad. Sci. U.S.A.* **2001**, *98*, 11265−11270.
(43) Stefl, R.; Trantirek, L.; Vorlickova, M.; Koca, J.; Sklenar, V.; Kypr, J. *J. Mol. Biol.* **2001**, *307*, 513−524.
(44) Krummel, A. T.; Mukherjee, P.; Zanni, M. T. *J. Phys. Chem. B* **2003**, *107*, 9165−9169.
(45) Hamm, P.; Lim, M.; Hochstrasser, R. M. *J. Phys. Chem. B* **1998**, *102*, 6123−6138.
(46) Kwiatkowski, J. S.; Leszczynski, J. *J. Phys. Chem.* **1996**, *100*, 941−953.
(47) Florian, J.; Baumruk, V.; Leszczynski, J. *J. Phys. Chem.* **1996**, *100*, 5578−5589.
(48) Brauer, B.; Gerber, R. B.; Kabelac, M.; Hobza, P.; Bakker, J. M.; Riziq, A. G. A.; de Vries, M. S. *J. Phys. Chem. A* **2005**, *109*, 6974−6984.
(49) Krimm, S.; Bandekar, J. *Adv. Protein Chem.* **1986**, *38*, 181−364.
(50) Torii, H.; Tasumi, M. *J. Raman Spectrosc.* **1998**, *29*, 81−86.
(51) Cheatum, C. M.; Tokmakoff, A.; Knoester, J. *J. Chem. Phys.* **2004**, *120*, 8201−8215.
(52) Hamm, P.; Woutersen, S. *Bull. Chem. Soc. Jpn.* **2002**, *75*, 985−988.
(53) Ham, S.; Cha, S.; Choi, J. H.; Cho, M. *J. Chem. Phys.* **2003**, *119*, 1451−1461.
(54) Carmona, P.; Molina, M. *J. Phys. Chem. B* **2000**, 104, 7496−7501.
(55) Elstner, M.; Hobza, P.; Frauenheim, T.; Suhai, S.; Kaxiras, E. *J. Chem. Phys.* **2001**, *114*, 5149−5155.
(56) Wu, Q.; Yang, W. T. *J. Chem. Phys.* **2002**, *116*, 515−524.
(57) Hobza, P.; Sponer, J. *J. Am. Chem. Soc.* **2002**, *124*, 11802−11808.
(58) Miyazawa, T. *J. Chem. Phys.* **1960**, *32*, 1647−1652.
(59) Bruinsma, R.; Gruner, G.; D′Orsogna, M. R.; Rudnick, J. *Phys. Rev. Lett.* **2000**, *85*, 4393−4396.
(60) Zhang, H. Y.; Li, X. Q.; Han, P.; Yu, X. Y.; Yan, Y. J. *J. Chem. Phys.* **2002**, *117*, 4578−4584.
(61) Ding, F.; Zanni, M. T. Manuscript in preparation.